Synthesis and Electrical Properties of the $Pr_{0.5+x-y}Bi_yLi_{0.5-3x}TiO_3$ System

María-Luisa Martínez-Sarrión,*[a] Lourdes Mestres,[a] Marta Herráiz,[a] Oscar Maqueda,[a] Nestor Fernández,[b] and Mario-Fidel García[c]

Keywords: Phase diagrams / Perovskite phases / Conducting materials

The stoichiometry, polymorphism, and electrical behaviour of the solid solutions $Pr_{0.5+x-y}Bi_yLi_{0.5-3x}TiO_3$ with perovskite-like structure have been studied. Data are given as a solid solution triangle, XRD patterns for two polymorphs T and O, the composition dependence of their parameters, and ionic conductivity plots. A region of perovskite-like solid solutions was obtained when the bismuth content in the general formula $Pr_{0.5+x-y}Bi_yLi_{0.5-3x}TiO_3$ was $y \leq 0.10$ and the lithium content was $0.033 \leq x \leq 0.133$. The compounds are mixed conductors. With increasing amounts of lithium the ionic conductivity first increased, reached a maximum for $x = 0.20$, with a conductivity at 25 °C of $6.639 \cdot 10^{-3}$ S·cm^{-1}, and then decreased.

Introduction

There has been much recent interest in the development of novel ionic conductors as solid electrolytes in lithium batteries.[1−12] Fast ionic conductors with the general formula $RE_{0.5+x}Li_{0.5-3x}TiO_3$, where RE = La, Pr, Nd, and Sm have been reported,[7−12] for which the maximum conductivity was for the La series ($1.1 \cdot 10^{-3}$ S·cm^{-1} for $x = 0.07$ at room temperature).[7] More recently the phase diagram, crystal chemistry, and ionic conductivity of the system $La_{0.5+x-y}Bi_yLi_{0.5-3x}TiO_3$ have been reported.[13] The compounds of this system are ionic conductors whose conductivity increases as the amount of lithium increases, up to $x = 0.075$, but decreases when the amount of bismuth increases. The system with Bi needs less time in the thirst treatment at 1250 °C than a similar system without bismuth.[13]

We aimed to investigate the stoichiometry range, crystal chemistry, and electrical behaviour of materials of the general formula $Pr_{0.5+x-y}Bi_yLi_{0.5-3x}TiO_3$ and to establish the phase diagram at room temperature of the system $Pr_{0.67}TiO_3/Pr_{0.5}Li_{0.5}TiO_3/Bi_{0.5}Li_{0.5}TiO_3$. XRD patterns of perovskites with different Li and Bi contents have been analyzed and a study of the thermal treatment time with the content of Bi made. Finally, electrical conductivity data have been interpreted on the basis of the structural information deduced.

Results and Discussion

Phase Diagram

The triangle $Pr_{0.67}TiO_3/Pr_{0.5}Li_{0.5}TiO_3/Bi_{0.5}Li_{0.5}TiO_3$ in the system $Pr_6O_{11}/Li_2O/TiO_2/Bi_2O_3$ was chosen for detailed study since the $Pr_{0.67}TiO_3/Pr_{0.5}Li_{0.5}TiO_3$ join has been previously reported.[12] Thus, compositions of general formula $Pr_{0.5+x+y}Bi_yLi_{0.5-3x}TiO_3$ were synthesized as described in the Exp. Sect. The results of X-ray powder diffraction were then used to construct the composition diagram shown in Figure 1. ICP analysis confirmed the nominal composition, and these results were then used to construct the diagram.

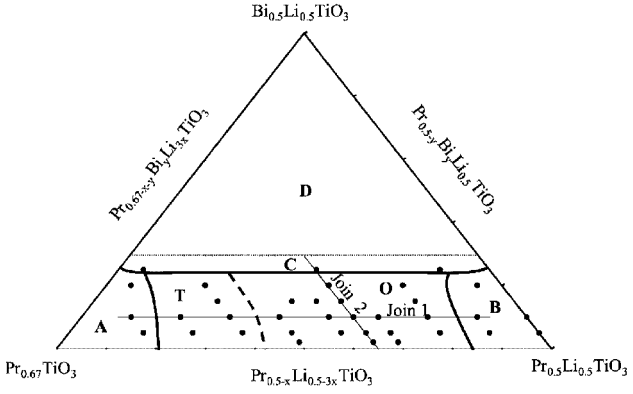

Figure 1. Composition triangle and joins studied for the system $Pr_{0.5+x-y}Bi_yLi_{0.5-3x}TiO_3$

[a] Departament de Química Inorgànica, Universitat de Barcelona, Martí i Franquès 1−11, 08028 Barcelona, Spain
Fax: (internat.) + 34-93/4907725
E-mail: marialuisa.martinez@qi.ub.es
[b] Departamento de Química Inorgánica, Universidad de La Habana,
Ciudad de la Habana, Cuba
[c] IMRE,
Ciudad de la Habana, Cuba

  DOI: 10.1002/ejic.200200657

Five distinct areas were found on this triangle: a region of perovskite-like solid solutions and three mixed-phase regions. Almost all of the superior part of the triangle (region C) was a mixture of the perovskite-like phase, $Bi_4Ti_3O_{12}$ (identified from PDF 73-2181) and an unknown phase (Figure 2, a). The region that was within the vertex $Pr_{0.5}Li_{0.5}TiO_3$ (region B) was a mixture of perovskite-like compound and peaks belonging to Li_2TiO_3, (identified from PDF 33-0831) (Figure 2, b), while the region close to the vertex $Pr_{0.67}TiO_3$ (region A) was a mixture of a perovskite-like phase and $Pr_4Ti_9O_{24}$ (identified from PDF 45-0265) (Figure 2, e). However, a perovskite-like solid solutions area (regions O and T) was also found between these three regions (Figure 2, c and d). No use was made of the previous results for $La_{0.5+x-y}Bi_yLi_{0.5-3x}TiO_3$[13] to study higher bismuth contents here (area D) as melting occurs because of the greater content of bismuth as Bi_2O_3, which melts at about 830 °C.

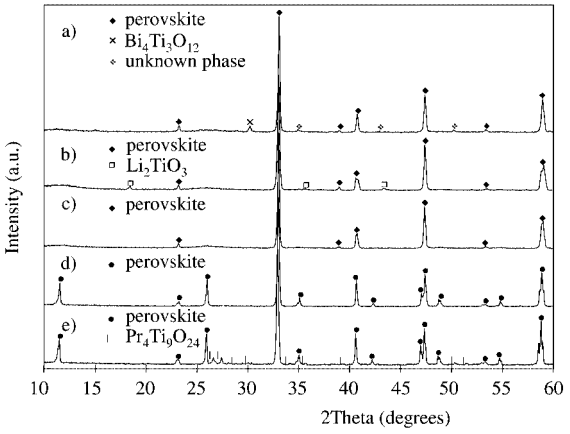

Figure 2. XRD patterns of the five regions on the composition triangle, showing both tetragonal (d) and orthorhombic (c) perovskite-like phases

Table 1 shows the X-ray powder diffraction data for $Pr_{0.57}Bi_{0.05}Li_{0.15}TiO_3$ (region T), which has a tetragonal perovskite-type structure. Table 2 shows the X-ray diffraction data for $Pr_{0.51}Bi_{0.05}Li_{0.325}TiO_3$ (region O), an orthorhombic perovskite-type structure. These two polymorphs are similar to those described in the $RE_{0.5+x}Li_{0.5-3x}TiO_3$ (RE = Pr, Nd) systems.[10,12]

Table 3 shows the X-ray diffraction data for $Pr_{0.58}Bi_{0.05}Li_{0.10}TiO_3$ (region A), containing reflections corresponding to a tetragonal perovskite-like structure and reflections corresponding to $Pr_4Ti_9O_{24}$. Table 4 shows the X-ray powder diffraction data for $Pr_{0.48}Bi_{0.025}Li_{0.5}TiO_3$ (region B) for which reflections corresponding to an orthorhombic perovskite-type structure and reflections corresponding to Li_2TiO_3 were observed. Finally, Table 5 shows X-ray powder diffraction data for $Pr_{0.43}Bi_{0.125}Li_{0.325}TiO_3$ (region C). In this region reflections corresponding to an orthorhombic perovskite-type structure, $Bi_4Ti_3O_{12}$, and an unknown phase were detected.

Perovskite-like phases mixed with titanium compounds are obtained in the areas A and B. In the area close to the

Table 1. Indexed powder pattern of the single-phase $Pr_{0.57}Bi_{0.05}Li_{0.15}TiO_3$ [tetragonal system: a = 3.833(8) Å, c = 7.721(2) Å, V = 113.48(6) Å^3, Z = 4]

hkl	$d_{obsd.}$ [Å]	$d_{calcd.}$ [Å]	I/I_o
001	7.671	7.721	21
100	3.843	3.834	4
011	3.427	3.434	24
102	2.718	2.720	100
111	2.556	2.558	8
112	2.219	2.219	23
013	2.138	2.137	3
004	1.931	1.930	12
020	1.917	1.917	28
113	1.869	1.866	4
202	1.722	1.717	2
121	1.673	1.674	4
114	1.573	1.572	14
122	1.569	1.567	29

Table 2. Indexed powder pattern of the single-phase $Pr_{0.51}Bi_{0.05}Li_{0.325}TiO_3$ [orthorhombic system: a = 5.434(3) Å, b = 7.674(4) Å, c = 5.415(1) Å, V = 225.83(7) Å^3, Z = 4]

hkl	$d_{obsd.}$ [Å]	$d_{calcd.}$ [Å]	I/I_o
101	3.835	3.836	5
121	2.714	2.713	100
112	2.312	2.311	2
220	2.219	2.218	13
022	2.214	2.212	14
040	1.919	1.918	37
222	1.717	1.716	3
123	1.565	1.564	24

Table 3. Indexed powder pattern of $Pr_{0.58}Bi_{0.05}Li_{0.10}TiO_3$

$d_{obsd.}$ [Å]	Perovskite d [Å]	*hkl*	$Pr_4Ti_9O_{24}$ d [Å]	*hkl*
7.705	7.671	001		
3.859	3.843	100		
3.434	3.427	011		
3.358			3.355	440
3.255			3.258	044
3.028			3.036	353
2.979			2.980	391
2.950			2.946	193
2.722	2.718	102		
2.625			2.629	115
2.560	2.556	111		
2.515			2.521	404
2.292			2.288	602
2.222	2.219	112		
2.141	2.138	013		
1.937	1.931	004		
1.919	1.917	020		
1.866	1.869	113		
1.812			1.814	800
1.775	1.720	202		
1.718			1.717	4106
1.677	1.673	121		
1.576	1.573	114		
1.570	1.569	122		

Table 4. Indexed powder pattern of $Pr_{0.48}Bi_{0.025}Li_{0.5}TiO_3$

$d_{obsd.}$ [Å]	Perovskite		Li_2TiO_3	
	d [Å]	hkl	d [Å]	hkl
4.798			4.800	002
3.827	3.835	101		
2.706	2.714	121		
2.511			2.502	−131
2.309	2.312	112		
2.216	2.219	220		
2.209	2.214	022		
2.075			2.075	−133
1.915	1.919	040		
1.714	1.717	222		
1.566	1.565	123		

Table 5. Indexed powder pattern of $Pr_{0.43}Bi_{0.125}Li_{0.325}TiO_3$

d_{obs} [Å]	Perovskite		$Bi_4Ti_3O_{12}$	
	d [Å]	hkl	d [Å]	hkl
3.827	3.835	101		
2.954			2.970	117
2.710	2.714	121		
2.563[a]				
2.309	2.312	112		
2.214	2.214	022		
2.108[a]				
1.917	1.919	040		
1.815[a]				
1.714	1.717	222		
1.566	1.565	123		

[a] Unknown phase.

vertex $Pr_{0.67}TiO_3$ (region A), $Pr_4Ti_9O_{24}$ is segregated along with the perovskite-like phase. On progressing towards the join $Pr_{0.67}TiO_3/Pr_{0.5}Li_{0.5}TiO_3$ the lithium content increases and Li_2TiO_3 is segregated along with the perovskite-like phase near the $Pr_{0.5}Li_{0.5}TiO_3$ vertex (region B).

The cell volume was obtained for two joins on the composition triangle (Figure 1). Along join 1 [$Pr_{0.45+x}Bi_{0.05}Li_{0.5-3x}TiO_3$] the lithium and praseodymium composition and the number of vacancies changed and the composition of bismuth was constant, while along join 2 [$Pr_{0.558-y}Bi_yLi_{0.325}TiO_3$] the number of vacancies and the amount of lithium was constant.

The cell volume was plotted against the amount of bismuth or lithium (Figure 3, a and b, respectively) and was found to increase smoothly as the bismuth content increased; conversely, it decreased smoothly with increasing lithium content. The bismuth, praseodymium, and lithium should be in equivalent 12-coordinated sites. Substitution of praseodymium by bismuth does not affect considerably the cell parameters due to their similar ionic radius. Therefore, the substitution of praseodymium by lithium leads to a reduction of the cell volume because the lithium ionic radius is smaller.

Electrical Measurements (AC)

DC conductivity measurements were carried out, but electronic conductivity was not found in these compounds.

AC measurements were carried out from 25 to 300 °C for compounds on join 1, $Pr_{0.45+x}Bi_{0.05}Li_{0.5-3x}TiO_3$ ($0.033 \leq x \leq 0.133$), and join 2, $Pr_{0.558-y}Bi_yLi_{0.325}TiO_3$ ($y \leq 0.10$). Two semicircles and a spike were observed in the impedance complex plane plots (Figure 4). The centers of the semicircles were clearly depressed below the baseline, indicating the kind of non-Debye response that has been detected in other ionic conductors.[14−16]

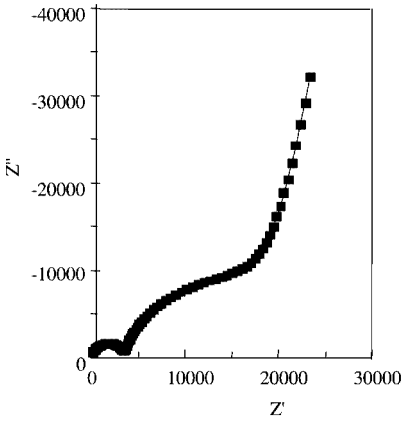

Figure 4. Impedance response at 155 °C for $Pr_{0.59}Bi_{0.01}Li_{0.325}TiO_3$

An equivalent circuit (Figure 5) with two RC elements and with CPE[16] (constant phase elements) for grain and

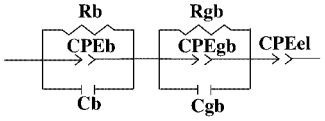

Figure 5. Equivalent circuit for fitting AC data and fitting results for $Pr_{0.59}Bi_{0.01}Li_{0.325}$ TiO_3 at 155 °C [Rb = 3535 Ω·cm, Cb = 9.12 10^{-12} F·cm^{-1}, Tb = 1.55 10^{-10} S·cm^{-1}, n = 0.88; Rgb = 15996 Ω·cm, Cgb = 2.41 10^{-9} F·cm^{-1}, Tgb = 5.37 10^{-10} S·cm^{-1}, n = 0.71; Tel = 9.37 10^{-10} S·cm^{-1}, n = 0.90; CPE equation: $Y = T\cdot\cos(n\pi/2)\cdot\omega^n + T\cdot\sin(n\pi/2)\cdot\omega^n$]

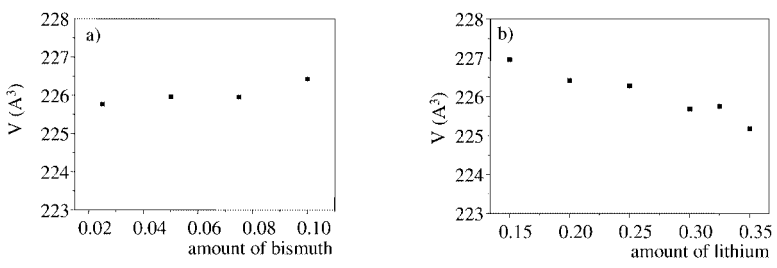

Figure 3. Cell volume with increasing concentration of a) bismuth and b) lithium

grain boundary response and an additional CPE element to model a low conductivity surface layer lithium ions was used to model the experimental data. All fitting used the Zview software package.[17] The first and second semicircles showed capacities of around 0.4 pF and 3 nF respectively, and are, therefore, related to bulk and grain boundaries. The spike had a capacitance around 30−60 nF, which is probably too small to be related to an electrode/sample double layer, but is probably linked to a low-conductivity layer on the pellet surface. Such a result has been reported for high Na^+ or Li^+ ion conductors[12−14] and attributed to the presence of an Na^+ or Li^+ free layer on the crystal surface.

Bulk ionic conductivity data from the impedance complex plane plots for compounds on joins $Pr_{0.45+x}Bi_{0.05}Li_{0.5-3x}TiO_3$ ($0.033 \leq x \leq 0.133$) and $Pr_{0.558-y}Bi_yLi_{0.325}TiO_3$ ($y \leq 0.10$) are shown in Arrhenius format in Figure 6 (a and b, respectively).

The variation in ionic conductivity with the increase of lithium concentration is quite large (Figure 7, a), while the activation energy is between 0.45 and 0.46 eV. No change in the conductivity mechanism can be supposed, but the increasing lithium concentration initially increases the concentration of carriers, thereby increasing the conductivity to a maximum at $x = 0.2$ with a conductivity at 25 °C of $6.639 \cdot 10^{-6}$ S·cm^{-1}. Further increases in the lithium concentration decreases the number of vacancies and the conductivity paths, with a corresponding decrease in conductivity. These results agree with earlier results for the La system,[13] which report a conduction mechanism based on the A-site vacancies.

Along the join $Pr_{0.558-y}Bi_yLi_{0.325}TiO_3$, where the amount of lithium remains constant, the conductivity decreases slightly when the amount of bismuth increases (Figure 7, b). However, substitution of Pr by Bi is not accompanied by a significant change in the cell volume of the perovskite, and so this behavior does not seem to be related to any change in the "bottleneck" size. However, it could be related to the lone-electron pair of bismuth.[18−19] The activation energy in this case was 0.45−0.46 eV.

Conclusions

A large range of single-phase solid solutions have been synthesized in the triangle $Pr_{0.67}TiO_3/Pr_{0.5}Li_{0.5}TiO_3/Bi_{0.5}Li_{0.5}TiO_3$. The phase diagram in the single-phase region showed the existence of two polymorphs with perovskite-like structures, labeled O and T. Polymorph O is an orthorhombic distortion of the simple cubic perovskite, while polymorph T is a tetragonal perovskite. Region A is a mixture of a perovskite-like phase and $Pr_4Ti_9O_{24}$. Region B is a mixture of a perovskite-like compound and Li_2TiO_3, and region C is a mixture of the perovskite-like phase, $Bi_4Ti_3O_{12}$ and an unknown phase.

The increase of bismuth concentration reduced the time for the third treatment and when $y \geq 0.075$ it is not necessary.

The cell volume decreased with increasing lithium content, but remained almost constant with increasing amounts of bismuth. This is attributable to the effect of ionic radii, which are similar for praseodymium and bismuth but shorter for lithium.

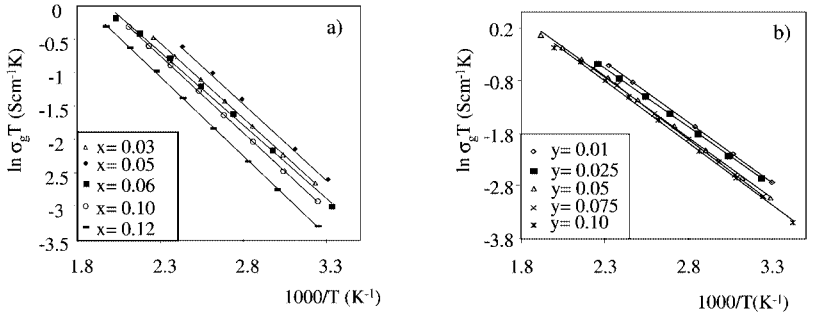

Figure 6. Arrhenius ionic conductivity plots for a) join 1 ($Pr_{0.45+x}Bi_{0.05}Li_{0.5-3x}TiO_3$) and b) join 2 ($Pr_{0.558-y}Bi_yLi_{0.325}TiO_3$)

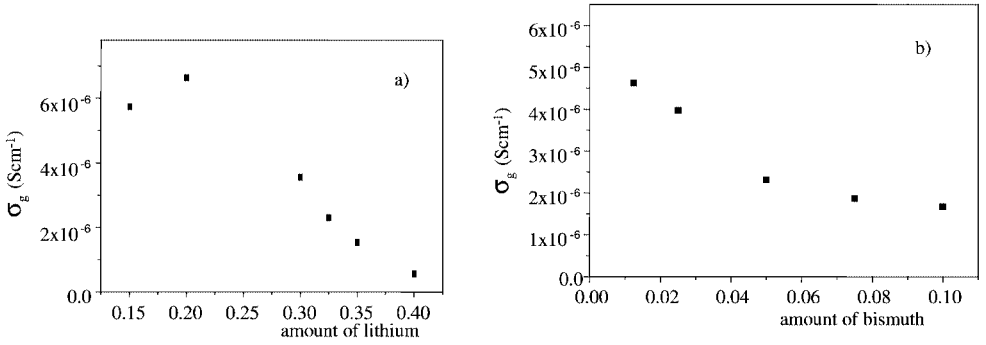

Figure 7. Plot of σ (bulk ionic conductivity) at room temperature vs. composition, a) in lithium along join 1 ($Pr_{0.45+x}Bi_{0.05}Li_{0.5-3x}TiO_3$) and b) in bismuth along join 2 ($Pr_{0.558-y}Bi_yLi_{0.325}TiO_3$)

AC/DC measurements indicated that these compounds are ionic conductors. Li^+ ion conductivity increased with increasing lithium content up to $x = 0.2$ and subsequently decreased; the conductivity decreased slightly with increasing bismuth concentration.

The behaviour of the $Pr_{0.5+x-y}Bi_yLi_{0.5-3x}TiO_3$ system is similar to that of the $La_{0.5+x-y}Bi_yLi_{0.5-3x}TiO_3$ system,[13] but, analogously to other systems of praseodymium, its ionic conductivity is lower than that of the corresponding lanthanum system.[3,5,20]

Experimental Section

Synthesis: Pr_6O_{11} (99.9%, Fluka), TiO_2 (99.9%, Aldrich), Bi_2O_3 (> 99%, J. T. Baker), and Li_2CO_3 (> 99%, Merck) were used as starting materials. Pr_6O_{11} and TiO_2 were dried overnight at 900 °C prior to weighing. Pretreated and untreated oxides were mixed in the desired proportions in an agate mortar with acetone, dried, and heated at 650 °C for 2 h to drive off CO_2. After grinding, samples were pressed into pellets, put into platinum vessels and covered with a powder of the same composition to avoid lithium loss during thermal treatment. The pellets were fired at 1100 °C for 12 h, giving green products that were reground, repelleted, and fired at 1200 °C for a further 12 h. A third treatment was carried out at 1250 °C, the required time depending on the Bi composition. Samples rich in Bi were found to need less time for the third treatment. Finally, the last treatment involved 4 h for samples with $y \leq 0.01$, 2 h for samples for $0.01 < y \leq 0.025$ and 1 h for samples of $0.025 < y \leq 0.05$. In samples with concentrations of bismuth of $y \geq 0.75$ no third treatment was necessary. After the third treatment, the samples were quenched in air to room temperature to stabilize the high-temperature phase.

X-ray Diffraction: The solid solution range, crystalline phase identification, and lattice parameters were obtained by powder X-ray diffraction with a Siemens D-500 diffractometer, in reflection mode, with a detector sensitive to the position and a secondary monochromator of quartz, using Cu-K_α radiation. Lattice parameters were obtained using a silicon internal standard.

ICP: Chemical analysis was performed by inductively coupled plasma (ICP) spectroscopy (Thermo Jarrel ASH Corporation, model Spectrometer Polyscan TM 61E) to determine the Li, Bi and Ti contents. The results indicated that the loss of lithium during firing was within the error range of the instrument; thus, the nominal composition is used here.

Electrical Measurements: DC conductivity measurements were carried out using an HP-34401A multimeter. AC measurements were performed with an HP 4192A Impedance Analyzer over the range $100\ Hz < f < 13\ MHz$, only in the single-phase region. Samples were pressed into pellets and sintered at 1250 °C for 1 h. Pellet sides were then sanded and painted with gold paste (Engelhard-Clal T-10112), which was fixed in a tubular furnace with a maximum temperature of 900 °C.

Acknowledgments

This work was partially sponsored by financial support from Ministerio de Ciencia y Tecnologia, Proyecto BQU2002-00619 and Generalitat de Catalunya, Proyecto 2001SGR00052.

[1] C. Julien, G. A. Nazri, in: *Solid State Bateries: Materials Design and Optimization*, Kluwer Academic Publishers, Dordrecht, **1994**.
[2] R. M. Dell, *Solid State Ionics* **2000**, *134*, 139−158.
[3] M. L. Martínez Sarrión, L. Mestres, M. Morales, M. Herraiz, *J. Solid State Chem.* **2000**, *155*, 280−285.
[4] M. L. Martínez Sarrión, L. Mestres, R. Palacín, M. Herraiz, *Eur. J. Inorg. Chem.* **2001**, 1139−1144.
[5] M. Morales, M. L. Martínez Sarrión, *J. Mater. Chem.* **1998**, *8*, 1583−1587.
[6] M. Itoh, Y. Inaguma, W. H. Jung, L. Chen, T. Nakamura, *Solid State Ionics* **1994**, *70/71*, 203−207.
[7] Y. Inaguma, L. Chen, M. Itoh, T. Nakamura, *Solid State Ionics* **1994**, *70/71*, 196−202.
[8] Y. Inaguma, L. Chen, M. Itoh, T. Nakamura, *Solid State Communications* **1993**, *86*, 689−693.
[9] H. Kawai, J. Kuwano, *J. Electrochem. Soc.* **1994**, *141*, L78−L79.
[10] A. D. Robertson, S. García Martín, A. Coats, A. R. West, *J. Mater. Chem.* **1995**, *5*, 1405−1412.
[11] J. M. S. Skakle, G. C. Mather, M. Morales, R. I. Smith, A. R. West, *J. Mater. Chem.* **1995**, *5*, 1807−1808.
[12] M. Morales, A. R. West, *Solid State Ionics* **1996**, *91*, 33−43.
[13] M. L. Martínez-Sarrión, L. Mestres, M. Herráiz, O. Maqueda, A. Bakkali, N. Fernández, *Eur. J. Inorg. Chem.* **2002**, 1794−1800.
[14] P. G. Bruce, A. R. West, D. P. Almond, *Solid State Ionics* **1982**, *7*, 57−60.
[15] A. K. Jonscher, J. M. Reau, *J. Mater. Sci.* **1978**, *13*, 563−570.
[16] A. K. Jonscher, in: *Dielectric Relaxation in Solids*, Chelsea Dielectric Press, London, **1983**.
[17] *Zview for Windows* (version 1.4), Scribner Assoc. Inc., Charlotesville, Virginia, USA.
[18] Ph. Lacorre, *Solid State Sciences* **2000**, *2*, 755−758.
[19] F. Goutenoire, O. Isnard, E. Suard, O. Bohnke, Y. Laligant, R. Retoux, P. Lacorre, *J. Mater. Chem.* **2001**, *11*, 119−124.
[20] M. Itoh, Y. Inaguma, W. Jung, T. Nakamura, *Solid State Ionics* **1994**, *70/71*, 203−207.

Received November 21, 2002

